7922 *Inorg. Chem.* **2009**, *48*, 7922–7930
DOI: 10.1021/ic900973d

Inorganic Chemistry
Article

Intramolecular Rotation of Iron(II) Dithiaethyneporphyrin Double-Decker Complex: ^{1}H NMR Studies

Anna Berlicka and Lechosław Latos-Grażyński*

Department of Chemistry, University of Wrocław, 50 383 Wrocław, Poland

Received May 18, 2009

The paramagnetic six-coordinated iron(II) 3,8,13,18-tetraaryldithiaethyneporphyrin $(ES_2P)_2Fe^{II}$ complexes of the double-decker type have been synthesized using iron pentacarbonyl as the metal source. The complex contains two porphyrinic macrocycles coordinated to the iron(II) in the sandwich-like fashion as determined by ^{1}H NMR. The ^{1}H NMR spectra of $(ES_2P)_2Fe^{II}$ have been examined in detail in the 180 − 366 K temperature range. Functional group assignments based on the selective deuteration, analysis of T_1 relaxation times and the NOESY experiment have been made at 313 and 210 K. The variable temperature ^{1}H NMR studies allowed to elucidate the dynamic behavior of $(ES_2P)_2Fe^{II}$ which involves rotation of dithiaethyneporphyrin rings around the metal ion. To account for the observed conformational rearrangements a cube, a square antiprism or a distorted triangular dodecahedron structure of $(ES_2P)_2Fe^{II}$ defined by the mutual orientation of two macrocyclic ligands have been considered. The six vertexes of a polyhedron are occupied by two pyrrolic nitrogens and four sulfur atoms, while two remaining vertexes are filled with two ethyne moieties. The dynamic rearrangements of $(ES_2P)_2Fe^{II}$ involve two enantiomeric couples of four fundamental staggered rotamers. The fast dynamic process engaging rotation of two dithiaethyneporphyrin ligands has been detected at 298 K. At low temperature range two rotamers have been identified as they presented the individual spectroscopic patterns. Considering the multiplicity of resonances the fast rotational oscillation involving one enantiomeric pair has been observed at 210 K, while all other processes are slow. The exchange between diastereomers has been confirmed at 210 K as the EXSY correlations linking diastereomeric resonances have been detected at the NOESY map.

Introduction

Metal ion bis(porphyrinate) or metal ion bis(phthalocyaninate) double-deckers contain the characteristic structural motif. Typically a large metal cation of charge +3, +4, or +5 is encompassed in a sandwich-like fashion by two negatively charged porphyrin and/or phthalocyanine ligands.[1−5] Such a coordination mode is a special feature of metal cations with large cationic radius, such as lanthanoids and actinoids, which do not closely fit to a coordination cavity of a macrocycle, forcing a displacement from the porphyrin plane after coordination, and in addition prefer higher coordination numbers.[6−9] Still, the double-deckers containing tetrapyrrole ligands can be formed by main groups metals and the transition metals providing that central metal ions bear high cationic charge.[3] Double-decker systems have caught special attention owing to unique electronic and redox properties associated with the strong $\pi-\pi$ interaction between two facing porphyrin-(phthalocyanine) macrocycles.[9−14]

*To whom correspondence should be addressed. E-mail: llg@wchuwr.pl.

(1) Buchler, J. W.; De Cian, A.; Fischer, J.; Kihn-Botulinski, M.; Paulus, H.; Weiss, R. *J. Am. Chem. Soc*. **1986**, *108*, 3652–3659.
(2) Buchler, J. W.; Hammerschmitt, P.; Kaufeld, I.; Loffler, J. *Chem. Ber*. **1991**, *124*, 2151–2159.
(3) Buchler, J. W.; Ng, D. K. P. Metal Tetrapyrrole Double- and Triple-Deckers with Special Emphasis on Porphyrin Systems; In *The Porphyrin Handbook*; Kadish, K. M., Smith, K. M., Guilard, R., eds. Academic Press: San Diego, CA, 2000; Vol. *3*, Chapter 21; pp 245-294.
(4) Ng, D. K. P.; Jiang, J. *Chem. Soc. Rev*. **1997**, *26*, 433–442.
(5) Jiang, J.; Ng, D. K. P. *Acc. Chem. Res*. **2009**, 79–88.
(6) Spyroulias, G. A.; Raptopoulou, C. P.; de Montauzon, D.; Mari, A.; Poilblanc, R.; Terzis, A.; Coutsolelos, A. G. *Inorg. Chem*. **1999**, *38*, 1683–1696.
(7) Guilard, R.; Barbe, J.-M.; Ibnlfassi, A.; Zrineh, A.; Adamian, V. A.; Kadish, K. M. *Inorg. Chem*. **1995**, *34*, 1472–1481.
(8) Zhang, X.; Muranaka, A.; Lv., W.; Zhang, Y.; Bian, Y.; Jiang, J.; Kobayashi, N. *Chem.—Eur. J*. **2008**, *14*, 4667–4674.
(9) Kadish, K. M.; Maninot, G.; Hu, Y.; Ibnlfassi, A.; Barbe, J. M.; Guilard, R. *J. Am. Chem. Soc*. **1993**, *115*, 8153–8166.
(10) Buchler, J. W.; Scharbert, B. *J. Am. Chem. Soc*. **1988**, *110*, 4272–4276.
(11) Bilsel, O.; Rodriguez, J.; Holten, D.; Girolami, G. S.; Milam, S. M.; Suslick, K. S. *J. Am. Chem. Soc*. **1990**, *112*, 4075–4077.
(12) Bilsel, O.; Rodriguez, J.; Milam, S. N.; Gorlin, P. A.; Girolami, G. S.; Suslick, K. S.; Holten, D. *J. Am. Chem. Soc*. **1992**, *114*, 6528–6538.
(13) Lu, F.; Sun, X.; Li, R.; Liang, D.; Zhu, P.; Choi, C.-F.; Ng, D. K. P.; Fukuda, T.; Kobayashi, N.; Bai, M.; Ma, C.; Jiang, J. *New J. Chem*. **2004**, *28*, 1116–1122.
(14) Girolami, G. S.; Gorlin, P. A.; Suslick, K. S. *Inorg. Chem*. **1994**, *33*, 626–627.

Published on Web 07/13/2009

Chart 1. Dithiaethyneporphyrins **1**

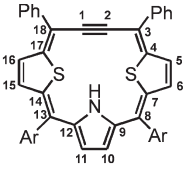

1-1 Ar = Tol
1-2 Ar = Ph
1-3 Ar = (*p*-OMe)Ph

The specific conformational (rotational) flexibility of double-deckers has been of particular interest as well. To explore such rearrangements, the cerium(IV) and zirconium(IV) sandwich-like complexes have been extensively studied applying the variable-temperature ^{1}H NMR.[15−22] Interestingly, the ligand rotation was detected for D_2 chiral cerium(IV) and zirconium(IV) sandwich-like complexes using chirality as a probe.[20] Several structural and electronic factors control the rotational freedom of the porphyrin units in double-deckers: (a) an ionic radius of the central metal atom, (b) bulkiness of the *meso*-aryl substituents, (c) a redox state and the protonation of porphyrin ligands, (d) a concentration of Ag(I) ions because of the host−guest-type chemical interactions.[22,23] These features are considered as suitable intra- and intermolecular switches of conformational activity.

In general rotating molecules including metalloporphyrin double-deckers are interesting in view of the design of recognition systems, molecular rotors, information transfer/storage devices.[23−27] Thus several rotating molecular and supramolecular systems have been reported to date.[17,22,28−30] Altogether, the formation of double-decker complexes have been practically limited to metalloporphyrins or metallophthalocyanines.

Previously we have reported the synthesis and characterization of 3,8,13,18-tetraaryl-19,21-dithiaethyneporphyrin (ES_2P)H, **1**.[31] This porphyrinoid (Chart 1) is a peculiar type

Chart 2. Double-decker complexes **2**

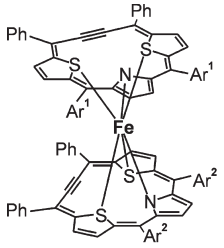

2-1 $Ar^1 = Ar^2$ = Tol
2-2 $Ar^1 = Ar^2$ = Ph
2-3 $Ar^1 = Ar^2$ = (*p*-OMe)Ph
2-4 Ar^1 = Ph, Ar^2 = (*p*-OMe)Ph

of contracted heteroporphyrin related to putative [18]triphyrin(4.1.1) with an acetylene moiety embedded in the macrocyclic framework. It introduces a unique structural pattern for contracted porphyrins, created by fusing the structural motifs of 21,23-dithiaporphyrin and acetylene. This macrocycle acts as a monoanionic ligand, which forms the five-coordinate ruthenium(II) complex.[31] Significantly acetylene fragment is not involved in coordination of the metal ion.

In this study, an insertion of iron(II) into **1** has been explored. For the very first time it has been demonstrated that contracted porphyrinoid−dithiaethyneporphyrin, as a ligand, allows a formation of the double-decker structures **2** (Chart 2). ^{1}H NMR spectroscopy was shown to be a definitive method for detecting and characterizing paramagnetic iron porphyrins,[32−34] iron *N*-substituted porphyrins,[35−39] or hemoproteins at different coordination/oxidation states,[40,41] as well as paramagnetic metallocarbaporphyrinoids.[42] In this contribution, ^{1}H NMR spectroscopy has been utilized as a suitable probe to explore the ligand rotational activities of the paramagnetic iron(II) dithiaethyneporphyrin complex allowing to identify two rotamers of its double-decker structure.

(15) Tashiro, K.; Konishi, K.; Aida, T. *Angew. Chem., Int. Ed. Engl.* **1997**, *36*, 856–858.
(16) Buchler, J. W.; H einz, G. *Chem. Ber.* **1996**, *129*, 201–205.
(17) Tashiro, K.; Fujiwara, T.; Konishi, K.; Aida, T. *Chem. Commun.* **1998**, 1121–1122.
(18) Buchler, J. W.; Eiermann, V.; Hanssum, H.; Heinz, G.; Ruterjans, H.; Schwarzkopf, M. *Chem. Ber.* **1994**, *127*, 589–595.
(19) Takeuchi, M.; Imada, T.; Ikeda, M.; Shinkai, S. *Tetrahedron Lett.* **1998**, *39*, 7897–7900.
(20) Tashiro, K.; Konishi, K.; Aida, T. *J. Am. Chem. Soc.* **2000**, *122*, 7921–7926.
(21) Ikeda, M.; Takeuchi, M.; Shinkai, S.; Tani, F.; Naruta, Y. *Bull. Chem. Soc. Jpn.* **2001**, *74*, 739–746.
(22) Ikeda, M.; Takeuchi, M.; Shinkai, S.; Tani, F.; Naruta, Y.; Sakamoto, S.; Yamaguchi, K. *Chem.—Eur. J.* **2002**, *8*, 5541–5550.
(23) Ikeda, M.; Tanida, T.; Takeuchi, M.; Shinkai, S. *Org. Lett.* **2000**, *2*, 1803–1805.
(24) Hembury, G. A.; Borovkov, V. V.; Inoue, Y. *Chem. Rev.* **2008**, *108*, 1–73.
(25) Ercolani, G. *Org. Lett.* **2005**, *7*, 803–805.
(26) Takeuchi, M.; Imada, T.; Shinkai, S. *Angew. Chem., Int. Ed.* **1998**, *37*, 2096–2099.
(27) Sugasaki, A.; Ikeda, M.; Takeuchi, M.; Robertson, A.; Shinkai, S. *J. Chem. Soc. Perkin Trans.1* **1999**, 3259–3264.
(28) Yanagisawa, M.; Tashiro, K.; Yamasaki, M.; Aida, T. *J. Am. Chem. Soc.* **2007**, *129*, 11912–11913.
(29) Otsuki, J.; Kawaguchi, S.; Yamakawa, T.; Asakawa, M.; Mizuno, Y. *Langmuir* **2006**, *22*, 5708–5715.
(30) Takami, T.; Ye, T.; Arnold, D. P.; Sugiura, K.; Wang, R.; Weiss, P. S. *J. Phys. Chem.C* **2007**, *111*, 2077–2080.
(31) Berlicka, A.; Latos-Grażyński, L.; Lis, T. *Angew. Chem., Int. Ed.* **2005**, *44*, 5288–5291.
(32) Walker, F. A. Proton NMR and EPR Spectroscopy of Paramagnetic Metalloporphyrins; In *The Porphyrin Handbook*; Kadish, K. M., Smith, K. M., Guilard, R., eds. Academic Press: San Diego, CA, 2000; Vol.*5*, Chapter 36; pp 81-183.
(33) Nakamura, Y.; Aratani, N.; Shinokubo, H.; Takagi, A.; Kawai, T.; Matsumoto, T.; Yoon, Z. S.; Kim, D. Y.; Ahn, T. K.; Kim, D.; Muranaka, A.; Kobayashi, N.; Osuka, A. *J. Am. Chem. Soc.* **2006**, *128*, 4119–4127.
(34) Baldini, L.; Ballester, P.; Casnati, A.; Gomila, R. M.; Hunter, C. A.; Sansone, F.; Ungaro, R. *J. Am. Chem. Soc.* **2003**, *125*, 14181–14189.
(35) Balch, A. L.; Cornman, C. R.; Latos-Grażyński, L.; Olmstead, M. M. *J. Am. Chem. Soc.* **1990**, *112*, 7552–7558.
(36) Balch, A. L.; Cornman, C. R.; Latos-Grażyński, L.; Renner, M. W. *J. Am. Chem. Soc.* **1992**, *114*, 2230–2237.
(37) Balch, A. L.; La Mar, G. N.; Latos-Grażyński, L.; Renner, M. W. *Inorg. Chem.* **1985**, *24*, 2432–2436.
(38) Balch, A. L.; Chan, Y.-W.; La Mar, G. N.; Latos-Grażyński, L.; Renner, M. W. *Inorg. Chem.* **1985**, *24*, 1437–1443.
(39) Wysłouch, A.; Latos-Grażyński, L.; Grzeszczuk, M.; Drabent, K.; Bartczak, T. *J. Chem. Soc., Chem. Commun.* **1988**, 1377–1378.
(40) La Mar, G. N.; Satterlee, J. D.; De Ropp, J. S. Nuclear Magnetic Resonance of Hemoproteins; In *The Porphyrin Handbook*; Kadish, K. M., Smith, K. M., Guilard, R., eds. Academic Press: San Diego, CA, 2000; Vol. *5*, Chapter 37; pp 185-298.
(41) Banci, L.; Bertini, I.; Luchinat, C.; Turano, P. Solutions Sturctures of Hemoproteins; In *The Porphyrin Handbook*; Kadish, K. M., Smith, K. M., Guilard, R., eds. Academic Press: San Diego, CA, 2000; Vol. *5*, Chapter 39; pp 323-350.
(42) Pacholska-Dudziak, E.; Latos-Grażyński, L. *Eur. J. Inorg. Chem.* **2007**, 2594–2608.

Scheme 1. Synthesis of **2**-1

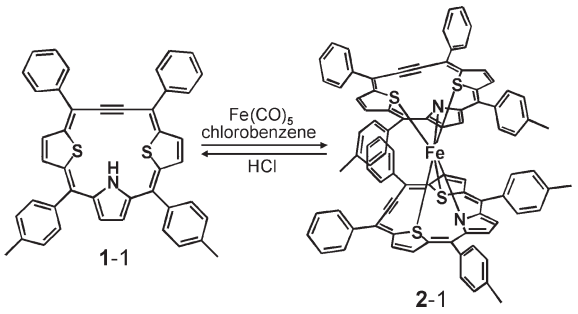

Results and Discussion

Synthesis of Iron(II) Dithiaethyneporphyrin. Insertion of iron into 3,18-diphenyl-8,13-di(*p*-tolyl)dithiaethyneporphyrin **1**-1 has been carried out by refluxing the ligand and large excess of iron pentacarbonyl in chlorobenzene solution under a nitrogen atmosphere. The process is accompanied by decomposition of $Fe(CO)_5$ to the metallic iron. The reaction yields a paramagnetic, six-coordinated iron(II) dithiaethyneporphyrin complex $(ES_2P)_2$-Fe^{II} **2**-1 of the double-decker type as a sole metallopophyrinoid product (Scheme 1). The resulting complex **2**-1 has good solubility in dichloromethane and chloroform and moderate solubility in tetrahydrofuran and toluene. In the solid state **2**-1 is stable to the atmosphere. Solutions of the iron(II) complex are stable toward atmospheric oxidation, but they undergo gradual demetalation in the presence of acid eventually giving free macrocycle **1**-1. Thus the insertion of iron(II) resulted in formation of the unprecedented double-decker system where iron(II) is encompassed in a sandwich-like fashion by two negatively charged dithiaethyneporphyrins. The macrocycle interior is too tight to accommodate the metal ion so the double-decker formation is preferable (Scheme 1).

The absorption spectrum of **2**-1 shows a single intense broad Soret band at 449 nm and two very weak bands in the visible region (Figure 1). The Soret band is at the same position as for corresponding dithiaethyneporphyrin **1**-1, while the Q bands demonstrate a bathochromic shift.

The electrochemical behavior of the homoleptic double-decker **2**-1 was studied by cyclic voltammetry. The reversible oxidation at −26 mV (vs Fc/Fc^+) corresponds to oxidation of the metal center.

The stoichiometry of **2**-1 was unambiguously confirmed by high resolution mass spectrometry (HRMS, ESI; *m*/*z* calcd for $[C_{88}H_{60}N_2S_4Fe]^+$, M^+: 1328.2987; found: 1328.2922). The formation of a sandwich-like complex of iron(II) has been supported by additional experiment. The reaction of $Fe(CO)_5$ and an equimolar mixture of two dithiaethyneporphyrins sufficiently differentiated by peripheral substitution, that is, 3,8,13,18-tetraphenyldithiaethyneporphyrin **1**-2 and 3,18-diphenyl-8,13-bis(*p*-metoxyphenyl)dithiaethyneporphyrin **1**-3 is expected to produce a set of two homoleptic **2**-2 (Fe(**1**-2)$_2$) and **2**-3 (Fe(**1**-3)$_2$) and one heteroleptic **2**-4 (Fe(**1**-2)(**1**-3)) species providing that the double-decker structure is properly recognized. The characteristic pattern descended exclusively from heteroleptic complex **2**-4 has been readily detected in the mass spectrum (ESI; *m*/*z* calcd for the major isotopomer $[C_{86}H_{56}N_2S_4O_2Fe]^+$, $[Fe(\mathbf{1}\text{-}2)(\mathbf{1}\text{-}3)]^+$: 1332; found:1332).

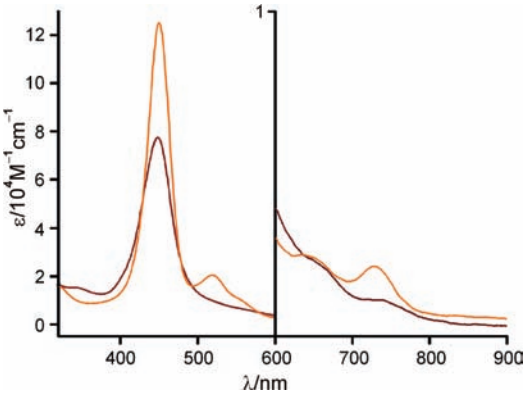

Figure 1. Absorption spectra of **1**-1 (orange) and **2**-1 (red) in CH_2Cl_2 at 298 K.

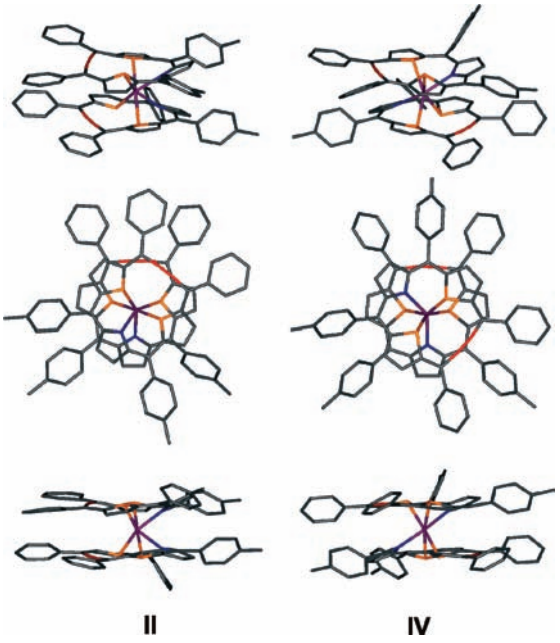

Figure 2. Drawing of two staggered rotamers of **2**-1 obtained from the molecular mechanics calculations: the vicinal **II** and transversal **IV** conformers, respectively.

Molecular Model of 2. Extensive attempts to obtain **2**-*n* as crystals, suitable for X-ray crystallographic studies, have not been successful. In the absence of such a data set, molecular mechanics calculations have been used to visualize the structures of two fundamental rotamers of the double-decker complex and to access the degree of the porphyrin distortion that is necessary to form this species (Figure 2). In the minimization procedure we have used the standard MM+ parametrization of the HyperChem program with an exception of the iron coordination surroundings where we have imposed the constraints reflecting the high-spin state of the iron(II) ion applying the respective data determined previously for iron(II) 21-thiaporphyrin.[43] The characteristic features included long iron−nitrogen (2.127 Å) and iron−sulfur (2.388 Å)

(43) Latos-Grażyński, L.; Lisowski, J.; Olmstead, M. M.; Balch, A. L. *Inorg. Chem.* **1989**, *28*, 1183–1188.

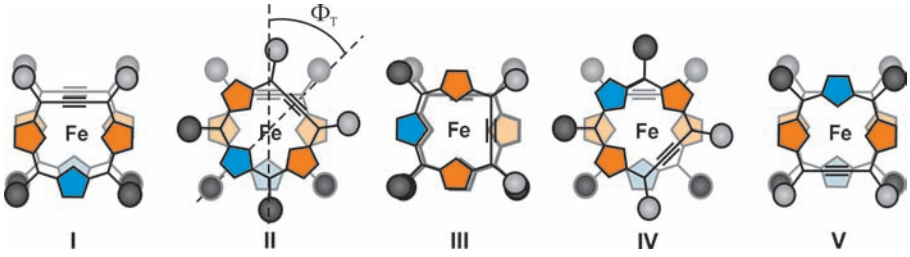

Figure 3. Projection along the main rotational axis of two dithiaethyneporphyrin rings in iron(II) double-decker complex **2**-1. The front porphyrin is black, while the rear one is gray. The two nonequivalent types of *meso*-aryls are marked by black and gray circles. The "twist angle" ϕ_T is the angle of rotation of one ring away from the eclipsed conformation of the two rings.

bonds. Characteristic pyramidal side-on coordination of the thiophene ring to the metal ion has been also postulated.[43−46] Additionally the thiophene rings in each of the ligands must be tilted in the same direction.

Altogether the double-deckers **2**-*n* have a six-coordinate metal ion that is bound to two nitrogens atoms and four thiophene sulfurs in a roughly trigonal antiprism arrangement. It is important to recognize that two fundamental rotamers are differentiated by mutual orientation of two basal triangle faces. Nevertheless, to simplify our analysis of the ^{1}H NMR data, we have adopted a different approach to represent the principal rotamers of **2**-1. Such a presentation mode was developed previously for metal tetrapyrrolic double-deckers. Thus, it was noted that eight pyrrole nitrogen atoms of porphyrinic rings may arrange into a cube, a square antiprism, or a distorted triangular dodecahedron structure depending on the mutual orientation of two macrocyclic ligands.[3] Our approach applied to describe the rearrangements of **2**-1 implies the coordination number eight for iron(II) which is actually quite rare for this metal ion. Subsequently it has been assumed that six vertexes of an appropriate polyhedron are occupied by two pyrrolic nitrogens and four sulfur atoms which form the regular coordination bonds. Two remaining vertexes are filled with two ethyne moieties which do not coordinate in a regular sense but occupy the space around central metal ion allocated by a polyhedron choice.

To distinguish possible conformers of homoleptic double-deckers **2**, so-called "twist angle" ϕ_T has been used. This angle acquires the value 0° for cubic, 45° for the square antiprismatic, and in between these values for the distorted dodecahedral structure.[3] The representative rotamers of **2**-1, which differ by $\phi_T = 45°$, are shown in Figure 3. Actually this angle might adopt several values between 0° and 180° (0° and −180°) as shown in Figure 3. One can expect that the staggered conformers: vicinal **II** and transversal **IV** with "twist angle" $\phi_T = -45°$, 45° and $\phi_T = -135°$, 135° respectively are the most stable because of the minimized steric hindrance of *meso*-aryl substituents. Such considerations are consistent with the known crystal structures of metal bisporphyrin complexes, which adopt the square antiprismatic geometry.[1,6,13,47,48]

Assignment of ^{1}H NMR Resonances. A representative ^{1}H NMR spectrum of iron(II) dithiaethyneporphyrin **2**-1 at 313 K is presented in Figure 4A. The spectrum was collected at 313 K to achieve the best resolution. The spectroscopic pattern is consistent with the high-spin character of iron(II) complex ($S = 2$; $(d_{xy})^2(d_{xz},d_{yz})^2(d_{z^2})^1(d_{x^2-y^2})^1$), resembling the essential features determined for ^{1}H NMR spectra of monomeric high-spin five-coordinated iron(II) core modified porphyrinoids.[38,49−54] The assignments, which are given above selected peaks (Figure 4), have been made on the basis of paramagnetic shifts, site-specific deuteration, analysis of T_1 values and 2D NOESY map. To identify pyrrole and aryl resonances, the ^{1}H NMR spectra of deuterated analogues **2**-2-d_x (partially pyrrole deuterated) and **2**-2-d_{20} (3,18-phenyl and 8,13-phenyl deuterated) have been synthesized. The chemical shifts and T_1 values of well separated signals of **2**-1 at 313 and 210 K are reported in Table 1.

The ^{1}H NMR data at 313 K have been analyzed on the presumption of effective C_{2v} or C_i symmetry of **2**-1, resulting from conformational interconversions (Figure 3). In such a case two distinct thiophene and one pyrrole resonances are expected. The phenyl and *p*-tolyl *meso* substituents are pairwise equivalent as well. Because of the double-decker structure, two *ortho* and two *meta* positions of *meso*-aryls will be distinguishable by ^{1}H NMR unless a rotation around C_{meso}-C_{ipso} bond is sufficiently fast. It is also significant that such a fast rotation has been definitely excluded in the case of *meso*-*p*-tolyls but remains unrestricted for *meso*-phenyls in the whole investigated temperature range (see below).

Two downfield shifted peaks at 28.7 and 27.3 ppm, and two upfield shifted resonances at −19.2 and −35.2 ppm have been observed at 313 K (Figure 4A). The relative intensity of each of these signals corresponds to

(44) Latos-Grażyński, L.; Lisowski, J.; Olmstead, M. M.; Balch, A. L. *J. Am. Chem. Soc.* **1987**, *109*, 4428–4429.
(45) Latos-Grażyński, L.; Lisowski, J.; Olmstead, M. M.; Balch, A. L. *Inorg. Chem.* **1989**, *28*, 3328–3331.
(46) Hung, C.-H.; Ou, C.-K.; Lee, G.-H.; Peng, S.-M. *Inorg. Chem.* **2001**, *40*, 6845–6847.
(47) Wang, R.; Li, R.; Liang, D.; Zhang, X.; Zhu, P.; Lo, P.-C.; Ng, D. K. P.; Pan, N.; Ma, C.; Kobayashi, N.; Jiang, J. *Chem.—Eur. J.* **2006**, *12*, 1475–1485.
(48) Spyroulias, G. A.; Coutsolelos, A. G.; Raptopoulou, C. P.; Terzis, A. *Inorg. Chem.* **1995**, *34*, 2476–2479.
(49) Latos-Grażyński, L. Core Modified Heteroanalogues of Porphyrins and Metalloporphyrins; In *The Porphyrin Handbook*; Kadish, K. M., Smith, K. M., Guilard, R., eds. Academic Press: New York, 2000; Vol. *2*, Chapter 14; pp 361-416.
(50) Pawlicki, M.; Latos-Grażyński, L. *Inorg. Chem.* **2004**, *43*, 5564–5571.
(51) Pawlicki, M.; Latos-Grażyński, L. *Inorg. Chem.* **2002**, *41*, 5866–5873.
(52) Rachlewicz, K.; Wang, S.-L.; Peng, C.-H.; Hung, C.-H.; Latos-Grażyński, L. *Inorg. Chem.* **2003**, *42*, 7348–7350.
(53) Rachlewicz, K.; Wang, S.-L.; Ko, J.-L.; Hung, C.-H.; Latos-Grażyński, L. *J. Am. Chem. Soc.* **2004**, *126*, 4420–4431.
(54) Rachlewicz, K.; Gorzelańczyk, D.; Latos-Grażyński, L. *Inorg. Chem.* **2006**, *45*, 9742–9747.

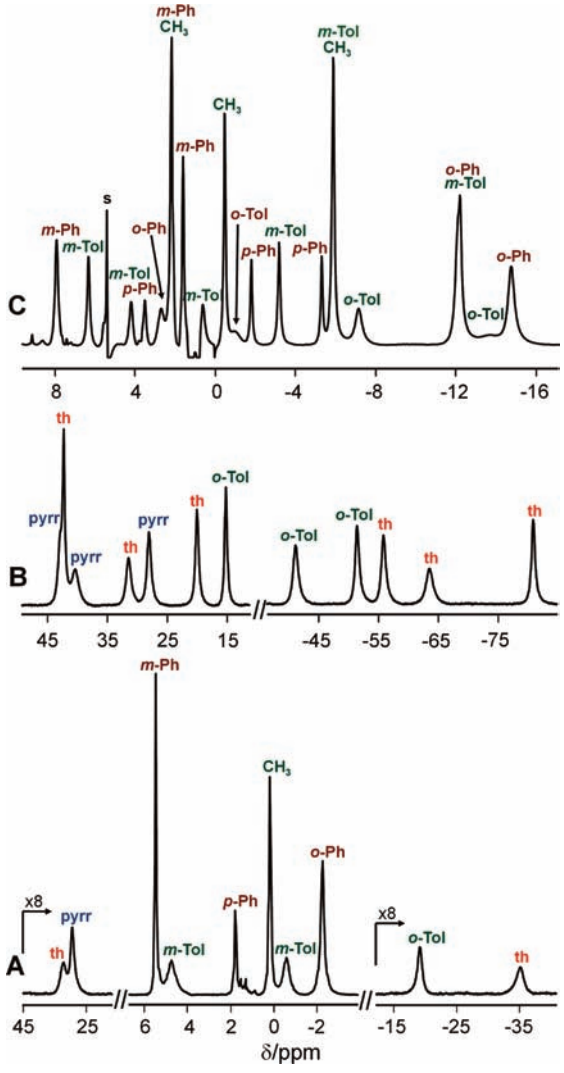

Figure 4. 600 MHz ^{1}H NMR spectra of the double-decker complex **2**-1 in CD_2Cl_2. The spectra have been obtained using the inversion−recovery technique. Trace A shows the entire spectrum at 313 K. Trace B presents downfield and highfield resonances, and trace C the 8.5 to −16.5 region at 210 K. Resonance assignments: pyrr, pyrrole protons; th, thiophene protons; *o*-Ph, *m*-Ph and *p*-Ph, *ortho*-, *meta*- and *para*-phenyl protons, respectively; *o*-Tol and *m*-Tol, *ortho*- and *meta*-tolyl protons, respectively; CH_3, *p*-methyl protons of the tolyl.

four protons (Table 1). The β pyrrole resonance has been unambiguously identified at 27.3 since this signal lowers the intensity at the spectrum of the pyrrole deuterated **2**-2-d_x.

The well-resolved pattern of *meso*-aryls resonances has been also identified in the ^{1}H NMR spectrum of **2**-1 (Figure 4A). Introduction of deuterated phenyl substituents at two nonequivalent *meso* positions 3,18 and 8,13 of **2**-2 has been crucial for assignment of phenyl and tolyl signals of **2**-1. The *ortho*-H, *meta*-H, *para*-H, and *p*-CH_3 resonances of two different aryls can be readily distinguished by their different longitudinal relaxation times (Table 1), as the *ortho* protons are closer to the iron(II) ion and, hence, have shorter T_1 values than the *meta* protons. Thus the relatively narrow *para* and methyl resonances should have longest relaxation times because of the longest distance from the paramagnetic metal center. The broad strongly upfield shifted peak at −19.2 ppm (313 K) was assigned to *ortho*-tolyl on the basis of the shortest relaxation time (3.1 ms), while two narrower signals observed at 4.7 and −0.5 ppm were assigned to *meta*-tolyl positions. The *meta* protons signals have the same intensity as *ortho*-tolyl, thiophene, and pyrrole resonances. The presence of a pair of *endo* and *exo* oriented *meta* hydrogens of *meso*-tolyl substituents confirms the slow rotation of *p*-tolyl around the $C_{meso}-C_{ipso}$ bond. Only one line was detected for *ortho*-tolyl protons. The counterpart *ortho* signal is not visible presumably because of strong broadening and/or overlapping with others resonances. The relatively narrow line at 0.2 ppm has been assigned to the *p*-methyl group of *meso*-*p*-tolyl ring. A comparison of signal intensities reveals that this line has the triple intensity with respect to *ortho*-H and *meta*-H *p*-tolyl signals. The differentiation of *ortho* and *meta meso*-aryl substituents is typical for bisporphyrin double-decker compounds.[9,18,47,55−57] Three lines located in the diamagnetic range of the ^{1}H NMR spectrum of **2**-1 were assigned to the *meso*-phenyl rings. Thus, the resonances at −2.3, 5.4, and 1.8 ppm were identified based on analysis of the relative intensities and relaxations times as *ortho*-, *meta*- and *para*-phenyl protons, respectively (Table 1). The *ortho*- and *meta*-phenyl lines have twice the intensity of *para*-phenyl protons, while the latter has intensity of four protons. The presence of one set of resonances indicates the free rotation of the *meso*-phenyl groups because of proximity of the acetylene unit instead of pyrrolic moiety, which considerably lowers the steric hindrance. The most characteristic feature, the upfield peak at −35.2 ppm and downfield signal at 28.7 ppm were assigned by default to the thiophene moiety (Figure 4A). The assignment at 210 K (Figure 4B,C) has followed the similar strategy as that described in detail above for the spectrum collected at 313 K.

In fact, the ^{1}H NMR spectra of **2**-1 have been measured in 180−313 K temperature range. Curie plots for pyrrole, thiophene, *ortho*-phenyl, and *ortho*-tolyl resonances of the double-decker complex **2**-1 are given in Figure 5. While the chemical shifts show linear behavior in the studied temperature range, the intercepts extrapolated to $1/T = 0$ are rather far from the diamagnetic positions, which are estimated from the data for the ruthenium complex of **1**-2.[31] Actually the extremely strong broadening of all resonances has been observed when the temperature reached 260 K, at which all peaks completely disappeared. At 240 K the novel spectroscopic pattern has been recorded albeit a well resolved spectrum has eventually registered at 210 K (Figure 4B,C). Such temperature dependence indicates the conformational rearrangements of double-decker **2**-1, which involves a rotation of two dithiaethyneporphyrin rings around the iron(II).[15,17,20−22]

Relaxation Studies. The choice of structural model can be reinforced with a quantitative analysis of the relaxation times, which can yield approximate distances

(55) Davoras, E. M.; Spyroulias, G. A.; Mikros, E.; Coutsolelos, A. G. *Inorg. Chem.* **1994**, *33*, 3430–3434.
(56) Bertini, I.; Coutsolelos, A.; Dikiy, A.; Luchinat, C.; Spyroulias, G. A.; Troganis, A. *Inorg. Chem.* **1996**, *35*, 6308–6315.
(57) Babailov, S. P.; Coutsolelos, A. G.; Dikiy, A.; Spyroulias, G. A. *Eur. J. Inorg. Chem.* **2001**, 303–306.

Table 1. Chemical Shifts and T_1 Values for Selected Resonances of **2**-1 in CD_2Cl_2 at 313 and 210 K[a]

313 K			210 K		
assignment	chemical shift, ppm	T_1, ms	assignment	chemical shift, ppm	T_1, ms
thiophene	28.7	3.4	thiophene	31.7	1.1
thiophene	−35.2	2.4	thiophene	20.3	2.6
pyrrole	27.3	1.9	thiophene	−55.7	1.6
o-Tol	−19.2	3.1	thiophene	−63.4	0.7
m-Tol (*endo*)	4.7	24.9	thiophene	−80.7	1.8
m-Tol (*exo*)	−0.5	30.7	pyrrole	28.3	1.0
CH_3	0.2	92.4	*o*-Tol (*exo*)	15.5	2.7
o-Ph	−2.3	8.0	*o*-Tol (*exo*)	−7.1	2.6
m-Ph	5.4	53.5	*o*-Tol (*endo*)	−41.1	1.2
p-Ph	1.8	106.3	*o*-Tol (*endo*)	−51.3	1.4
			m-Tol (*endo*)	6.2	10.5
			m-Tol (*endo*)	4.1	11.1
			m-Tol (*exo*)	−3.2	14.8
			CH_3	−0.5	42.8
			o-Ph	−14.7	3.4
			m-Ph	7.8	24.1
			p-Ph	−1.8	41.9
			p-Ph	−5.3	36.5

[a] Chemical shifts of all resonances of **2**-1 are included in the Experimental Section.

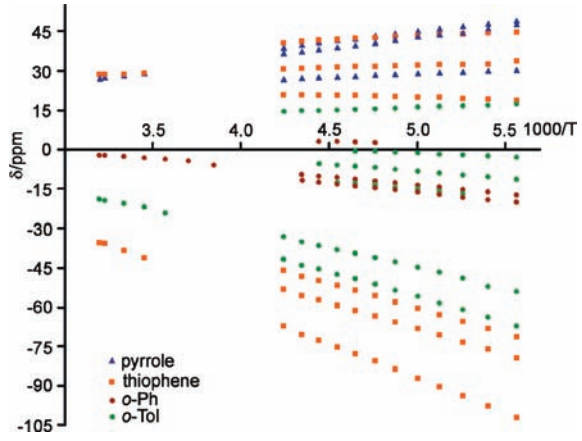

Figure 5. Curie plot for the pyrrole, thiophene, *o*-phenyl, and *o*-tolyl resonances of **2**-1 (CD_2Cl_2).

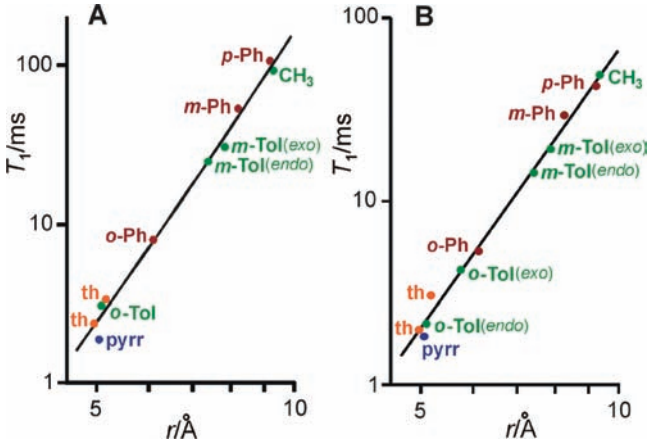

Figure 6. Relaxation plots for **2**-1 at 313 K (A) and 210 K (B). The dependence between T_1 (CD_2Cl_2) and r (model structure averages) is linear in bilogarithmic axes.

between the iron(II) ion and particular protons of **2**-1.[58,59] T_1 times are normally preferred to T_2, as they are independent of exchange phenomena.

Paramagnetically induced relaxation may be both of dipolar and scalar origin but the contact contribution (which can be estimated from chemical shifts) is small in **2**-1 and has been omitted in the calculations. Dipolar relaxation is expressed simply as

$$T_1 = a \cdot r^6 \qquad (1)$$

where r is the distance to the paramagnetic center, and a is a constant, which is equal for all the protons in the molecule. Equation 1 leads to a linear dependence between T_1 and r in bilogarithmic axes, with the slope equal to 6. Figure 6 shows the T_1 dependence on r for **2**-1. The r values are the averages of MM+ model distances. The resulting fits are fairly accurate.

(58) La Mar, G. N.; Walker, F. A. NMR of Paramagnetic Porphyrins; In *The Porphyrins*; Dolphin, D., ed. Academic Press: New York, 1979; pp 57-161.
(59) Bertini, I.; Luchinat, C. *Coord. Chem. Rev.* **1996**, *150*, 1–28.

Isotropic shifts. The complex molecular and electronic structure renders a complete analysis of the isotropic shifts unattainable. Nevertheless we have found that some features should be addressed. One has to realize that a contribution of the dipolar mechanism to the overall paramagnetic shifts of **2**-1 seems to be essential. Dominant dipolar shifts are determined by geometric factor and magnetic susceptibility tensor symmetry and its orientation with respect to the molecule,[32,58] both not determined for **2**-1. At present we can only comment that the *meso*-aryl resonances with exception of one (210 K) demonstrate negative isotropic shifts (the ruthenium(II) dithiaethyneporphyrin complex was used as the diamagnetic reference)[31] that are compatible with the dominance of the dipolar contribution at these particular positions.[32,58] Definitely the dipolar mechanism adds significantly to the total isotropic shifts of β pyrrole and thiophene hydrogens.

In spite of the obvious structural differences, the contact shifts of the double-decker high-spin iron(II) dithiathineporphyrin **2**-1 can be qualitatively related by

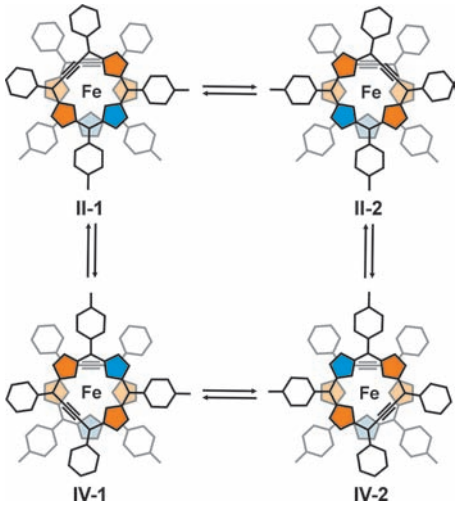

Figure 7. Representation of rearrangement mechanisms.

a spin density delocalization pattern typically exhibited by high-spin iron(II) porphyrins, iron(II) *N*-substituted porphyrins, iron(II) 21-heteroporphyrins, and iron(II) *N*-confused porphyrin.[32,38,38,42,51−54] Thus in the case of high-spin iron(II) center$-(d_{xy})^2(d_{xz}d_{yz})^2(d_{z^2})^1(d_{x^2-y^2})^1-$ both σ and π routes of spin density delocalization can operate. The pattern for the contact shift arises from the cancellation of effects of the unpaired spin density resulting from the spin delocalization in σ, as well as both filled and vacant π molecular orbitals. The contact shift predominates for the β-H pyrrole resonance yielding the downfield position.[32,38,51] Here the typical delocalization pathway involves the delocalization through a σ-framework by way of a σ-donation to the half occupied $d_{x^2-y^2}$ iron(II) orbital.[38] The spectroscopic distinctive feature of **2**-1 is the effect localized on the thiophene rings. In the case of β-H thiophene, resonances are evidently different from the pyrrolic ones presenting downfield and upfield positions. Thus the side on arrangement of the iron(II) with respect to the thiophene ring primarily affects π spin transfer producing the marked upfield relocation in a single thiophene position. Actually in paramagnetic complexes of 21-thiaporphyrin with nickel(II) and iron(II) the upfield shift of the thiophene resonances was related to the side-on binding mode. Such coordination allows direct spin density transfer from the metal ion to the thiaporphyrin π orbitals.[43,60] The analogous mechanism was involved for paramagnetic nickel(II) and iron(II) 2-aza-21-carbaporphyrins.[49,52−54,61]

Conformational Analysis. At the limiting and still hypothetical situation of completely frozen exchange processes of **2**-1 one can construct, because of the appropriate symmetry equivalence, the ^{1}H NMR spectrum of the **II-1**−**II-2** enantiomeric pair should be composed of four nonequivalent thiophene and two pyrrolic resonances. Accordingly two subset of six *meso*-phenyl and ten *meso*-tolyl resonances are generated presuming the rotation of *meso*-phenyl remains fast (Figure 8D). In fact the second enantiomeric couple **IV-1**−**IV-2** affords an analogous set

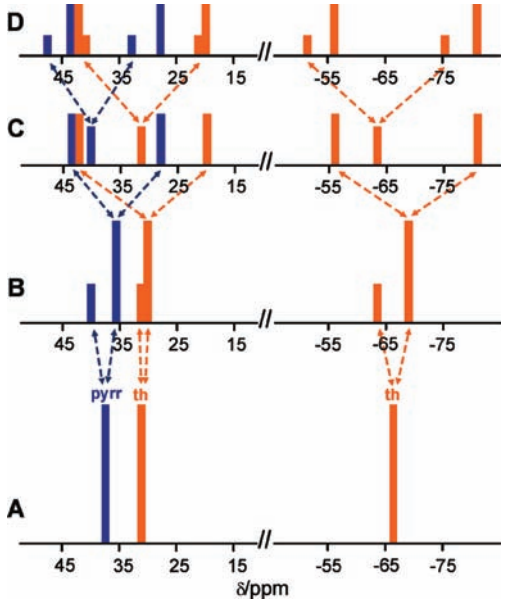

Figure 8. Schematic representation of the downfield and upfield region of the hypothetical ^{1}H NMR spectra (A−D) of **2**-1 at 210 K reflecting selected combinations of slow or fast exchange rates considered for interconversions between stereoisomers: (A) the free rotation around metal center (the positions of resonances extrapolated from 298 K); (B) the fast **II-1**⇄**II-2** (**IV-1**⇄**IV-2**) enantiomerization accompanied by the slow exchange between **II-1**⇄**IV-1** (**II-2**⇄**IV-2**) diastereomers, (C) the slow diastereomeric interconversion **II-1**⇄**IV-1** (**II-2**⇄**IV-2**) and enantiomeric oscillation **II-1**⇄**II-2** but the fast **IV-1**⇄**IV-2** enantiomerization. Alternatively the slow diastereomeric interconversion **II-1**⇄**IV-1** (**II-2**⇄**IV-2**) and enantiomeric oscillation **IV-1**⇄**IV-2** but the fast **II-1**⇄**II-2** enantiomerization. (D) The slow exchange between enantiomers and diastereomers. The experimental 2.7:1 molar ratio for two identified diastereomers has been accepted in whole analysis.

of resonances albeit of different chemical shifts. In fact the number of resonances recorded in the ^{1}H NMR spectrum (298 K−366 K) is markedly reduced and is consistent with the effective C_{2v} or C_i symmetry, which suggests the fast conformational rotation. The rearrangement process involves rotation or rotational oscillations which include four rotamers **II** and **IV** ($-45° \rightleftarrows 45° \rightleftarrows -135° \rightleftarrows 135° \rightleftarrows -45°$ etc.) (Figure 7).

The more complex scenario should be considered for the low temperature range where the selected exchange steps are significantly slower (Figure 8B−D). The dynamics of molecule **2**-1 have been analyzed as involving three fundamental intramolecular processes which should reveal different spectroscopic consequences once analyzed separately in fast exchange limit (Figure 7). Two of the processes involve rotational oscillation of vicinal **II-1** and **II-2**, and transversal **IV-1** and **IV-2** enantiomeric couples affording racemization. Consistently the pattern of resonances assigned respectively to **II**(**1**,**2**) or **IV**(**1**,**2**) enantiomeric pairs reduces to two nonequivalent thiophene and single pyrrolic resonances and two subset of three *meso*-phenyl and five *meso*-tolyl signals (Figure 8B). The slow dynamic equilibrium between diastereomers **II-1** and **II-2** or **IV-1** and **IV-2** will produce a single set composed from nonequivalent four thiophene and two pyrrolic resonances accompanied by two subsets of six *meso*-phenyl and ten *meso*-tolyl resonances (Figure 8C,D). Altogether one can consider eight different relations between the exchange rates presuming the

(60) Lisowski, J.; Latos-Grażyński, L.; Szterenberg, L. *Inorg. Chem.* **1992**, *31*, 1933–1940.
(61) Chmielewski, P. J.; Latos-Grażyński, L.; Głowiak, T. *J. Am. Chem. Soc.* **1996**, *118*, 5690–5701.

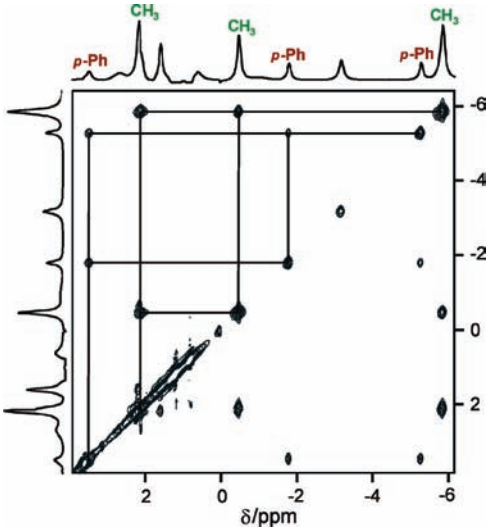

Figure 9. Fragment of ^{1}H NMR EXSY spectrum of **2**-1 (210 K, CD_2Cl_2, τ_M = 0.015 s). The exchange cross-peaks between *para*-phenyl and *p*-methyl tolyl peaks are shown. The exchange cross-peaks were also observed for related *meta*-phenyl and *meta*-tolyl resonances (Figure S3, Supporting Information). 1D spectrum has been obtained using the inversion−recovery technique.

given process is slow or fast in the NMR time scale. Accordingly, the hypothetic ^{1}H NMR spectra are given for pyrrole and thiophene resonances in Figure 8.

Actually, the ^{1}H NMR spectrum of **2**-1 in the 210 K range exhibits six thiophene and three pyrrole resonances (Figure 4B) which is consistent with the situation visualized at Trace C of Figure 8. Accordingly the conformational equilibrium involves the slow oscillation between isomers **II** ⇄ **IV** and **II-1** ⇄ **II-2** and the fast one involving the **IV-1** ⇄ **IV-2** oscillation. The alternative process involves the slow exchange between isomers **II** ⇄ **IV**, and **IV-1** ⇄ **IV-2** and the fast **II-1** ⇄ **II-2** rotational oscillation is feasible as well (Figure 7). The available experimental data do not allow to distinguish between these two rearrangement routes.

The fragment of the EXSY spectrum, shown in Figure 9, displays exchange correlations between corresponding *para*-phenyl and *p*-tolyl methyl signals of the two structurally different conformers yielding the picture which nicely corroborates with suggested dynamic processes. Additionally, the exchange cross-peaks are observed linking two different *meso*-phenyls and two *meso*-*p*-tolyl rings of the conformers in which the enantiomerization is in the slow exchange limit. These correlations facilitated an identification of signals in the crowded diamagnetic 0−3 ppm range. Significantly the connectivity between *endo* and *exo* pairs of *meta*-tolyl resonances has not been detected as expected for their frozen rotation.

One of the upfield shifted thiophene resonances is markedly broader than the two adjacent ones. Actually, an identical broadening pattern has been observed in the downfield region whereas one thiophene and one pyrrole resonance demonstrated dynamic broadening. These lines have been ascribed to the faster oscillating conformer **A**. Subsequently relative amounts of the two rotamers have been determined applying a careful deconvolution of the upfield thiophene region of the regular spectrum of **2**-1. The concentration ratio of the slow rotating conformer (**B**) to the second less abundant faster rotating isomer (**A**) determined at 210 K equals 2.7:1 (**A**, **B** not specifically assigned). In fact, two conformers **II** and **IV** are in thermodynamic equilibrium with the equilibrium constant K = [**B**]/[**A**] varying from 4.4:1 at 236 K to 1.6:1 at 180 K. The error of these estimations may exceed 10%. Approximate thermodynamic parameters received from these data are $\Delta H° = 5.8 \pm 0.3$ kJ/mol, $\Delta S° = 36.4 \pm 1.3$ J/mol·K (r^2 = 0.98) (Figure S2, Supporting Information).

The isotropic shift values corresponding to the slow exchange limit of **2**-1 can be readily extrapolated to 298 K whereas the fast rotation has been detected. Subsequently the exchange rate constant for the slow oscillating conformer has been evaluated to be higher than 2×10^4 s^{-1} (298 K) using the Gutowsky and Holm equation.[62] This value is considerably larger than those previously reported for cerium(IV) double-decker complexes (80−630 s^{-1} depending on the peripheral substitution).[15,17,22] This difference can be attributed to the lower steric hindrance caused by *meso*-aryls of **2**-1.

Conclusions

In the presented work, the unusual type of coordination for contracted porphyrinoids has been reported. Namely, the relatively small coordination core of dithiaethyneporphyrin induces the sandwich-like arrangement in the complex. In fact, the iron(II) bis(dithiaethyneporphyrin) is the first example of porphyrin double-decker complex reported for the transition metals of groups 6 to 11.

Till the present, the formation of double-decker complexes have been practically limited to metalloporphyrins or metallophthalocyanines. The analysis of the structural and electronic conditions which lead to formation of double-decker porphyrins suggests a new strategy to force the formation of such systems incorporating the first row (relatively small) transition metal(II) ions characterized by rather small tendency to acquire higher coordination numbers. Namely, it has been noted that tridentate macrocylic ligands including fused porphyrin can coordinate in the peculiar facial mode. Actually a specific orientation of large cation coordination polyhedron allows coordination to tridentate macrocycles which provide a relatively small coordination crevice as the three donor atoms are positioned at the vertices of the single trigonal face.[63−66] Significantly, such a coordination mode was considered for rhenium complexes of *N*-fused porphyrin,[67,68] ruthenium(II) complexes of dithiaethyneporphyrin[31] or dithiaethyneazuliporphyrin[69] and for [SiF_3(Me_3tacn)]Cl, where a distorted octahedral cation built upon facially

(62) Gutowsky, H. G.; Holm, C. H. *J. Phys. Chem.* **1956**, *25*, 1228–1231.
(63) Wainwright, K. P. *Coord. Chem. Rev.* **1997**, *166*, 35–90.
(64) Gott, A. L.; McGovan, P. C.; Temple, C. N. *Organometallics* **2008**, *27*, 2852–2860.
(65) Romakh, V. B.; Therrien, B.; Suss-Fink, G.; Shul'pin, G. B. *Inorg. Chem.* **2007**, *46*, 3166–3175.
(66) Che, C. M.; Ho, C. M.; Huang, J. S. *Coord. Chem. Rev.* **2007**, *251*, 2145–2166.
(67) Toganoh, M.; Ikeda, S.; Furuta, H. *Inorg. Chem.* **2007**, *46*, 10003–10015.
(68) Toganoh, M.; Ikeda, S.; Furuta, H. *Chem. Commun.* **2005**, 4589–4591.
(69) Berlicka, A.; Sprutta, N.; Latos-Grażyński, L. *Chem. Commun.* **2006**, 3346–3348.

coordinated Me_3tacn (*N*,*N*′,*N*″-trimethyl-1,4,7-triazacyclononane) and three fluoride ligands has been detected.[70] Generally, contracted monoanionic porphyrinoids coordinate forcing a large displacement of a central ion from the macrocylic plane as observed for rhenium *N*-fused porphyrin[67,68,71] or for *N*-fused porphyrin derivatives which incorporate small boron(III) or phosphorus(V).[72−74] In principle a sterically allowed coordination of the second porphyrinoid molecule may complete the double-decker formation. It remains to be explored if a emerging group of contracted three-dentate porphyrinoids including subporphyrins,[75−77] subpyriporphyrin,[78] [15]triphyrin(1.1.3),[79] and [14]triphyrin(2.1.1)[80] will provide a suitable environment for double-deckers of the transition metal ions.

Experimental Section

Materials. 3,18-Diphenyl-13,18-di(*p*-tolyl)-19,21-dithiaethyneporphyrin **1**-1, 3,8,13,18-tetraphenyl-19,21-dithiaethyneporphyrin **1**-2, and 3,18-diphenyl-13,18-bis(*p*-metoxyphenyl)-19,21-dithiaethyneporphyrin **1**-3 were obtained as described previously.[31] The deuterated analogues **1**-2-d_x (40% pyrrole deuterated as determined by ^{1}H NMR) and **1**-2-d_{10} (3,18-phenyl and 8,13-phenyl deuterated) were synthesized using pyrrole-d_5 or benzoyl chloride-d_5. Chlorobenzene was distilled over calcium hydride under nitrogen atmosphere prior to use.

Iron(II) Dithiaethyneporphyrin Double-Decker 2-1. Iron pentacarbonyl (6 mL, 45 mmol) was added in three portions over the course of 30 h (at 7−12 h intervals) to a refluxing solution of 3,18-diphenyl-8,13-di(*p*-tolyl)dithiaethyneporphyrin **1**-1 (20 mg, 0.032 mmol) dissolved in freshly distilled chlorobenzene (50 mL) under nitrogen atmosphere. The solvent was evaporated to dryness, and the solid residue was initially chromatographed on basic alumina column (grade III) with CH_2Cl_2 as eluent. The mixture of compounds was separated by the second chromatography on silica gel. The initial green fraction (iron claster) has been eluted with hexane and second orange (recovered porphyrin) with hexane/benzene (3:1 *V*/*V*), the elution with hexane/benzene (3:2 *V*/*V*) led to the third brown fraction, which was collected and identified as complex **2**-1. Recrystallization from CH_2Cl_2/hexane gives product in 30−50% yield. UV−vis, CH_2Cl_2 $\lambda(\log\varepsilon)$ = 449(4.9), 667(3.2), 742(2.8) nm; ^{1}H NMR (CD_2Cl_2, 313 K): δ = 28.7 (th); 27.3 (pyrr); 5.4 (*m*-Ph); 4.7 (*m*-Tol); 1.8 (*p*-Ph); 0.2 (CH_3 -Tol); −0.5 (*m*-Tol); −2.3 (*o*-Ph); −19.2 (*o*-Tol); −35.2 (th) ppm; ^{1}H NMR (CD_2Cl_2, 210 K): δ = 43.1 (pyrr); 42.6 (th); 40.7 (pyrr); 31.7 (th) 28.3 (pyrr); 20.3 (th); 15.5 (*o*-Tol); 7.8 (*m*-Ph); 6.2 (*m*-Tol); 4.1 (*m*-Tol); 3.5 (*p*-Ph); 2.6 (*o*-Ph); 2.2 (*m*-Ph, CH_3-Tol); 1.6 (*m*-Ph); 0.6 (*m*-Tol); −0.5 (CH_3-Tol); −0.9 (*o*-Tol); −1.8 (*p*-Ph); −3.2 (*m*-Tol); −5.3 (*p*-Ph); −5.9 (*m*-Tol, CH_3-Tol); −7.1 (*o*-Tol); −12.1 (*o*-Ph, *m*-Tol); −13.6 (*o*-Tol); −14.7 (o-Ph); −41.1 (*o*-Tol); −51.3 (*o*-Tol); −55.7 (th); −63,4 (th); −80.7 (th) ppm; HRMS (ESI, *m*/*z*): 1328.2922 (1328.2987 for $[C_{88}H_{60}N_2S_4Fe]^+$, M^+); elemental analysis: calcd (%) for $C_{88}H_{60}N_2S_4Fe\cdot 2.5CHCl_3\cdot 2.5C_6H_{14}$: C 68.74, H 5.33, N 1.52, S 6.96; found: C 68.40, H 4.99, N 1.73, S 6.91.

To identify pyrrole and aryl resonances, the ^{1}H NMR spectra of the deuterated analogues **2**-2-d_x (partially pyrrole deuterated) and **2**-2-d_{20} (3,18-phenyl and 8,13-phenyl deuterated) have been also obtained.

Instrumentation. The NMR spectra were recorded on a high-field spectrometer (^{1}H frequency 600.15 MHz) equipped with broadband inverse gradient probeheads. Spectra were referenced to the residual solvent signal (dichloromethane-d_2 5.32 ppm). Spectra were collected in 60,000−85,000 Hz spectral window with 16k data points with 500−4600 transients for the experiment and a 50 ms prepulse delay.

An inversion−recovery pulse sequence was used to suppress the diamagnetic signals in the spectra and to measure longitudinal relaxations times. The T_1 values were obtained from a two-parameter fit of the data to an exponential recovery function.

The EXSY spectrum was obtained using a conventional NOESY sequence with 2048 data points in the t_2 domain and 512 points in the t_1 domain, with a 50 ms recovery delay and a mixing time of 15 ms.

Absorption spectra were recorded on a diode array spectrometer. High resolution mass spectra were recorded using the electrospray mass spectrometry technique. One electron oxidation using DDQ facilitated mass spectrometry measurement. Electrochemical measurements were performed in dichloromethane with tetra-*n*-butylammonium perchlorate (TBAP) as a supporting electrolyte. Cyclic voltammetry was carried out with a conventional three-electrode system. A glassy carbon disk served as the working electrode, and a platinum wire was used as the counter electrode. The reference electrode was Ag/Ag^+. Redox potentials were determined with respect to ferrocene as an internal standard (E° = 0.406 V vs Ag/Ag^+).

Molecular Mechanics Calculation. Molecular mechanics calculations were performed using the HyperChem software (Autodesk). The standard MM+ force field, with the constraints set on the coordination bonds to achieve a high-spin iron(II) porphyrin geometry, were used as described in the text.

Acknowledgment. Financial support from the Ministry of Science and Higher Education (2015/W/WCh/09/6) is kindly acknowledged.

Supporting Information Available: Additional spectroscopic data This material is available free of charge via the Internet at http://pubs.acs.org.

(70) Cheng, F.; Hector, A. L.; Levason, W.; Reid, G.; Webster, M.; Zhang, W. J. *Chem. Commun.* **2009**, 1334–1336.
(71) Toganoh, M.; Ikeda, S.; Furuta, H. *Chem. Commun.* **2005**, 4589–4591.
(72) Pacholska-Dudziak, E.; Ulatowski, F.; Ciunik, Z.; Latos-Grażyński, L. *Chem. Eur. J.*, **2009**, in press.
(73) Młodzianowska, A.; Latos-Grażyński, L.; Szterenberg, L. *Inorg. Chem.* **2008**, *47*, 6364–6374.
(74) Młodzianowska, A.; Latos-Grażyński, L.; Szterenberg, L.; Stępień, M. *Inorg. Chem.* **2007**, *46*, 6950–6957.
(75) Saito, S.; Kim, K. S.; Yoon, Z. S.; Kim, D.; Osuka, A. *Angew. Chem., Int. Ed.* **2007**, *46*, 5591–5593.
(76) Inokuma, Y.; Kwon, J. H.; Ahn, T. K.; Yoo, M.-C.; Kim, D.; Osuka, A. *Angew. Chem., Int. Ed.* **2006**, *45*, 961–964.
(77) Kobayashi, N.; Takeuchi, Y.; Matsuda, A. *Angew. Chem., Int. Ed.* **2007**, *46*, 758–760.
(78) Myśliborski, R.; Latos-Grażyński, L.; Szterenberg, L.; Lis, T. *Angew. Chem., Int. Ed.* **2006**, *45*, 3670–3674.
(79) Krivokapic, A.; Cowley, A. R.; Anderson, H. L. *J. Org. Chem.* **2003**, *68*, 1089–1096.
(80) Xue, Z. L.; Shen, Z.; Mack, J.; Kuzuhara, D.; Yamada, H.; Okujima, T.; Ono, N.; You, X. Z.; Kobayashi, N. *J. Am. Chem. Soc.* **2008**, *130*, 16478–16479.